

## CHAPTER 3

### RESULTS AND DISCUSSION

#### 3.1 Development of soap bubble for gas sampling interface

##### 3.1.1 Requirements for soap bubble in gas sampling and analytical chemistry

In order for a soap bubble to be analytically useful as a gas sampling interface, it must have reproducible size and film thickness, and last a sufficiently long lifetime ( $> 10_{\text{min}}$ ). Such requirements can be met if the bubble is made from a constant volume of the soap solution using a constant amount of gas to inflate it. In order to make the soap bubble efficiently, the soap solution volume used should not exceed that required to make the desired size bubble. Otherwise, the excess soap solution will move due to gravity and accumulate as a drop at the bottom of the bubble and shorten its lifetime.

##### 3.1.2 Reproducibility of bubble size

The bubbles were created with a constant gas flow rate and a computerized timer. The bubble size was measured photographically with using a grid scale on the front panel of the box that is also reflected on a mirror placed on the panel behind the bubble such that parallax reading errors can be avoided. The bubble (made with 210 sccm gas flow for 5 s) was photographed immediately after formation with a high resolution digital camera and a sufficient depth of field that the photograph was

focused on both sides of the bubble, avoiding parallax as best as possible as shown in Figure 3.1. The bubble diameter, calculated from the difference of the left and right edge readings, was measured to be  $41.7 \pm 0.8$  mm ( $n=74$ , 1.9 %).

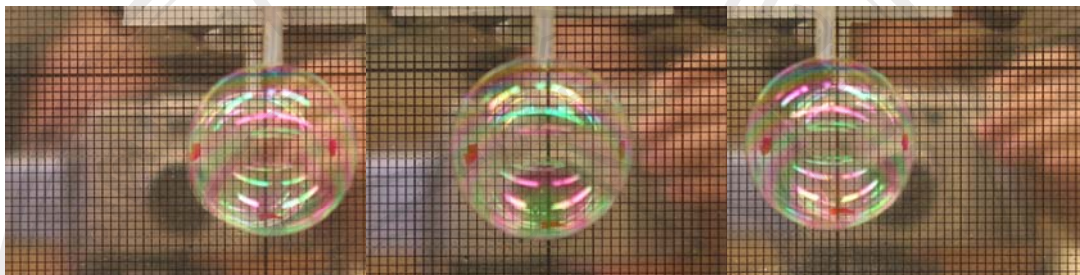


Figure 3.1 Photographic measurement of bubble size

### 3.1.3 Soap bubble film thickness

Bubble film thickness can be determined by comparing blue laser light (409 nm) absorbance, based on Lambert-Beer's Law, of yellow food dye in soap bubble and in thin quartz cell.

The bubble film thickness was measured by absorption spectroscopy under the same conditions as those in conductivity measurements; with the conductance electrodes touching the bubble during the optical measurement. Yellow food dye was added to the soap solution for making the bubble. A blue laser beam (409 nm) was directed through the bubble perpendicular to the axis connecting the electrodes, at the same vertical plane, as demonstrated in Figure 3.2. The transmitted light fell on a photodiode and the resulting current was converted to voltage by a current-voltage converter, and acquired on a computer. The absorbance value was calculated from the transmittance data after the usual logarithmic transformation.

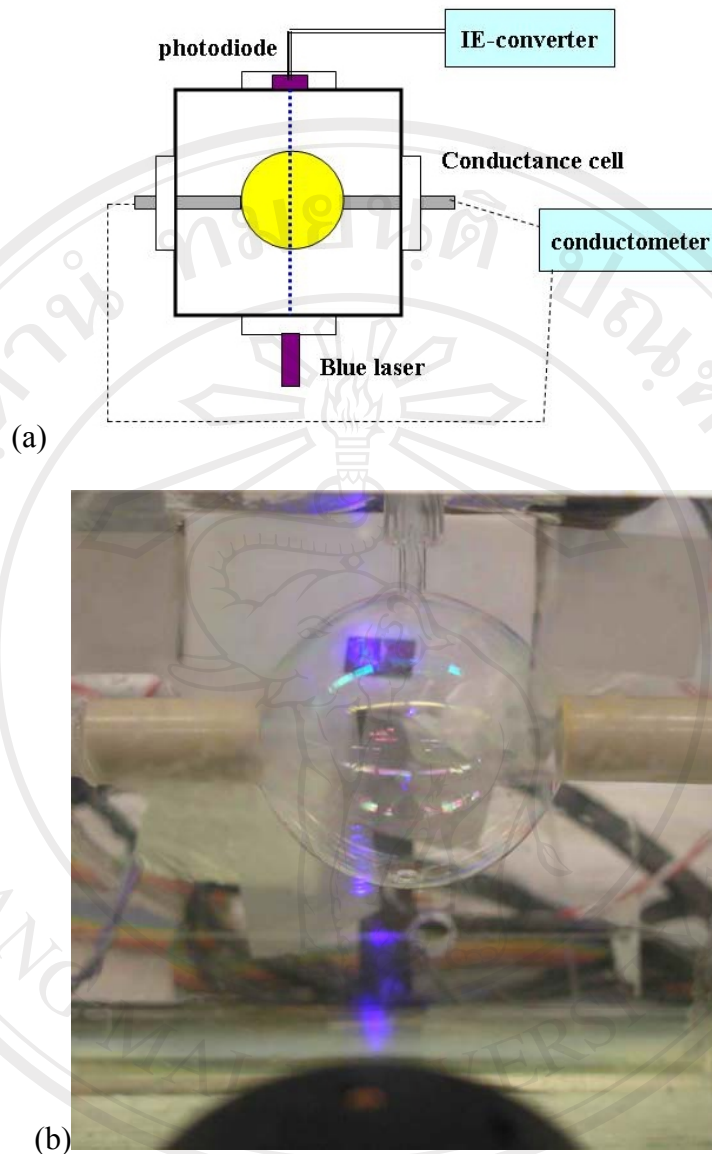


Figure 3.2 Soap bubble film thickness measurement setup. a) Top view of a chamber, b) a blue laser beam passes through the bubble perpendicular to the axis connecting the electrodes, at the same vertical plane

Having the bubble in contact with the electrodes during light transmission measurement interestingly results in a more stable transmittance photocurrent signal, presumably due to the inability of the bubble to move in that lateral direction. Henceforth, transmittance and conductivity measurements were simultaneously

carried out. The visible absorption band of yellow food dye in the TX-100-glycerol medium is very broad and is centered at 425 nm. As a result, measurements with a 409 nm laser and that by a conventional spectrometer at 409 nm (2 nm bandwidth) should be comparable. The visible wavelength spectrum of 0-10 % v/v of yellow food dye in purified 2% TX-100, 10% glycerol was measured in a cell of pathlength 103  $\mu\text{m}$ ; the spectra for the 1% and 10% dye solution are shown in Figure 3.3.

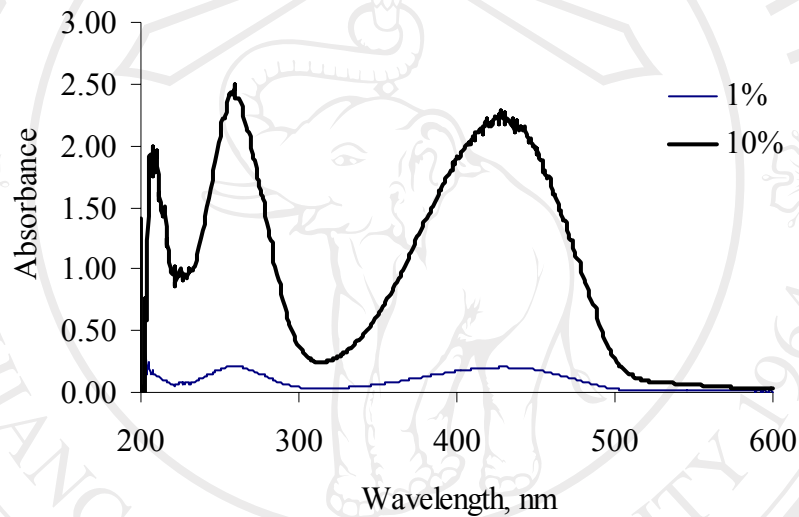


Figure 3.3 Absorption spectra of yellow food dye in a soap solution matrix, cell pathlength 103  $\mu\text{m}$

Others have reported that the bubble film thickness changes with time [110], also based on spectroscopic measurements. In our experiments, we also observed changes in bubble absorbance with time, as shown in Figure 3.4. The film thickness of the bubble must therefore be stated with specific reference to the age ( $\tau$ ) of the bubble (the bubbles remained attached to the bubble head for a period that generally

ranged from 15 to 18 min. After self-detachment from the bubble head, they still remained attached to the conductivity electrodes for a more extended period of time).

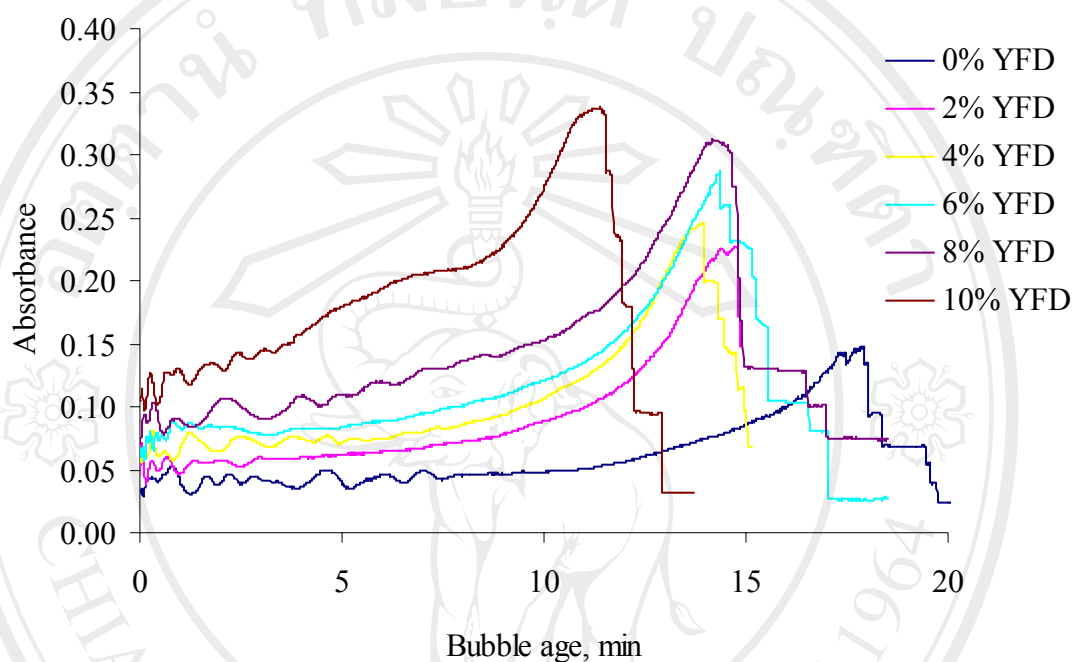


Figure 3.4 Temporal absorbance of soap bubble in various dye concentrations by using laser spectroscopy

Since the bubble film has a thickness of the  $\mu\text{m}$  order, relatively large concentrations of the dye must be added into the bubble making solution to get reliable absorbance measurements. We implicitly assume that the incorporation of the dye in the bubble film does not change its thickness significantly. The laser beam passes through the bubble wall twice. In the range of 2-6% dye concentration, both the conventional spectrophotometric measurement using the  $103 \mu\text{m}$  thin film cell and the bubble system obeyed Beer's law according to the following equations:

$$A_{103\mu\text{mcell}} = 0.0341(\pm 0.0675) + 0.169(\pm 0.0156) * [\text{YellowDye}, v/v\%], r^2 = 0.9916 \quad [3.1]$$

and

$$A_{\text{bubble}, \tau=5 \text{ min}} = 0.0106(\pm 0.0025) + 5.35(\pm 0.0156) * [\text{YellowDye}, v/v\%], r^2 = 0.9885 [3.2]$$

The bubble film thickness,  $\delta$ , at 5 min was calculated from the ratio of the slopes of eqns. [3.1] and [3.2], and the known path length (103  $\mu\text{m}$ ) of the conventional cell. In addition, the film thickness can be calculated from slope of a plot between the absorbance values measured in the two systems for the same set of solutions, as shown in Figure 3.5 for 0, 2, 4, 6, 8, and 10% dye solution; the line is drawn through the 2-6% concentration. It will be noted that at 8-10% dye concentrations the bubble absorbance is higher than that predicted by the behavior at lower dye concentrations. We believe that at these very high dye concentrations, the bubble film thickness actually increases. Also note that the dye concentration is referred to the stock dye solution as bought (which contains the FD&C Yellow 6 dye at an unspecified concentration in aqueous polypropylene glycol) in v/v and not in terms of the absolute dye content. The increase in thickness may be due to the glycol content of the dye solution.

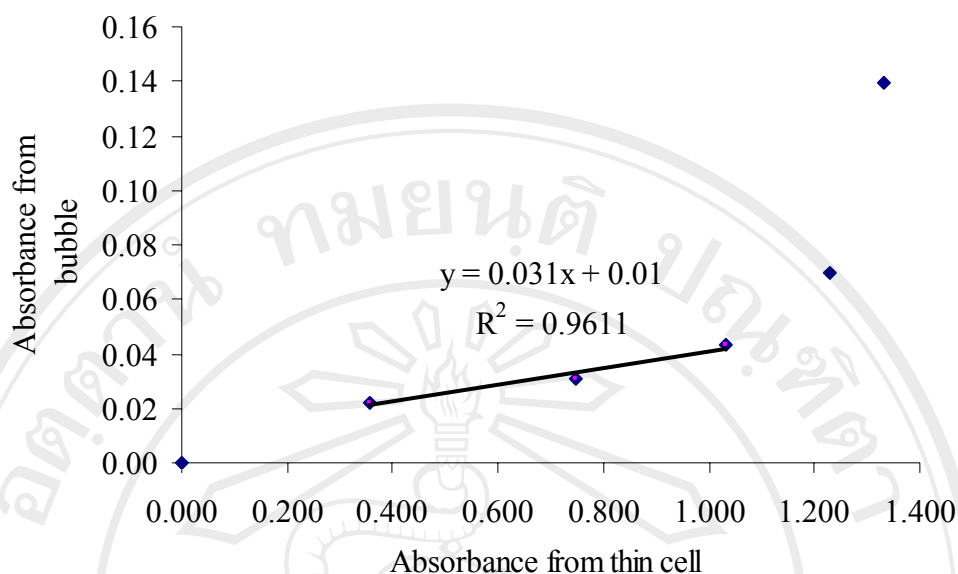


Figure 3.5 Absorbance of bubble and absorbance of bubble making solution from thin (103  $\mu\text{m}$  path length) cell. The slope of the line between 2-6% dye concentration was used for soap bubble film thickness calculation

The thin-cell pathlength was determined by calibration with KI solution at 227 nm in comparison with a standard 1.00 cm pathlength cell on the diode array spectrophotometer to be  $103 \pm 1.8 \mu\text{m}$ . Based on this therefore, bubble film thickness at 5 min,  $\delta\tau_{=5 \text{ min}}$  is  $1.6 \pm 0.2 \mu\text{m}$ .

From geometrical consideration of bubble, film thickness can be calculated from the equation:

$$\delta_{geom} = \frac{V_s}{4\pi r_b^2} \quad [3.3]$$

Where  $V_s$  is the volume of the bubble making solution delivered to the bubblehead. If 5  $\mu\text{L}$  of liquid is used to make a hollow bubble 3 cm in diameter, the

calculated wall thickness is 1.8  $\mu\text{m}$ . The film thickness obtained from optical measurement is thus of the same order of magnitude as that obtained from geometrical considerations.

### 3.2 Conductance in spherical soap bubble

The spherical soap bubble was performed and conductance of hollow film of such bubble was studied. The change of conductance of bubble, which added with  $\text{H}_2\text{SO}_4$  in bubble making solution, was investigated.

#### 3.2.1 Decreasing of conductance with time

Temporal conductance profiles of bubbles containing different amount of  $\text{H}_2\text{SO}_4$  with  $\pm 1$  standard deviation indicated as an error bar are shown in Figure 3.6. The average ( $n = 5-7$ ) conductance of a bubble containing various concentrations of  $\text{H}_2\text{SO}_4$  reproducibly decreases with time. This is because the film thickness decreases with time - gravity drags solution from the bubble wall to form a drop at the bottom of the bubble. Equation 3.4 can explain the observed experimental data. As may be intuitive, the conductance  $G$  (the derivation details of equation 3.4 is given in Appendix A) is directly proportional to the film thickness,  $\delta$ . The change in the bubble wall thickness thus directly affects the observed conductance.

$$G = \frac{\pi\delta\sigma}{\ln\left(\cot\frac{r_e}{2r_b}\right)} \quad [3.4]$$

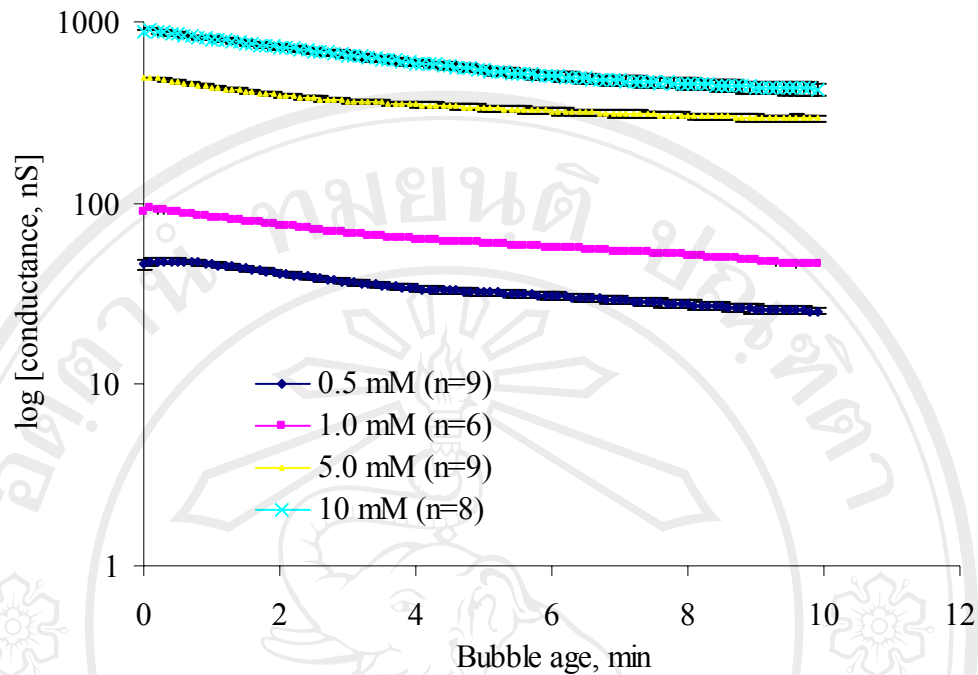


Figure 3.6 Temporal conductance profiles for bubbles containing various concentrations of  $\text{H}_2\text{SO}_4$

### 3.2.2 Conductance vs concentration

From the results in Figure 3.6, at any specific point in time, the conductance values are linearly correlated with the  $\text{H}_2\text{SO}_4$  concentration in the soap solution; this is depicted in Figure 3.7. The linear relationships between conductance vs. acid concentration at different times are shown below:

$$G_{\tau=0 \text{ min}, \text{ nS}} = 11.2 \pm 21.9 + 88.1 \pm 3.9 [\text{H}_2\text{SO}_4, \text{ mM}], r^2 = 0.9961 \quad [3.5]$$

$$G_{\tau=1 \text{ min}, \text{ nS}} = 11.3 \pm 14.8 + 80.5 \pm 2.6 [\text{H}_2\text{SO}_4, \text{ mM}], r^2 = 0.9979 \quad [3.6]$$

$$G_{\tau=5 \text{ min}, \text{ nS}} = 17.7 \pm 27.5 + 54.3 \pm 4.9 [\text{H}_2\text{SO}_4, \text{ mM}], r^2 = 0.9840 \quad [3.7]$$

$$G_{\tau=9 \text{ min}, \text{ nS}} = 18.8 \pm 33.4 + 44.4 \pm 5.9 [\text{H}_2\text{SO}_4, \text{ mM}], r^2 = 0.9654 \quad [3.8]$$

The slope of conductance vs. sulfuric acid concentration decreased exponentially with time; the logarithm of the slope values in equation 3.5 to 3.8 was linearly related to measuring time  $\tau$  with an  $r^2$  value of 0.9770 as in Figure 3.8.

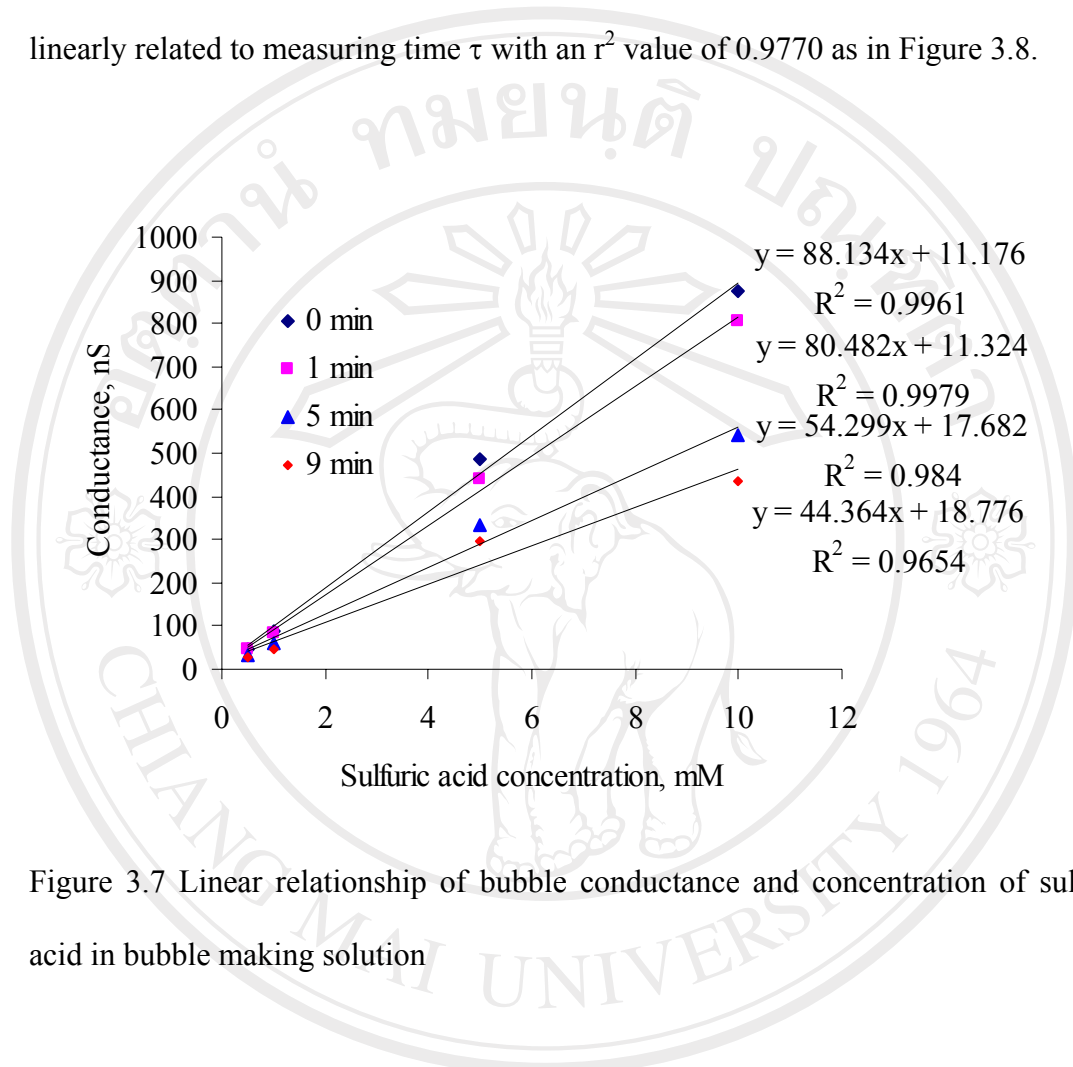


Figure 3.7 Linear relationship of bubble conductance and concentration of sulfuric acid in bubble making solution

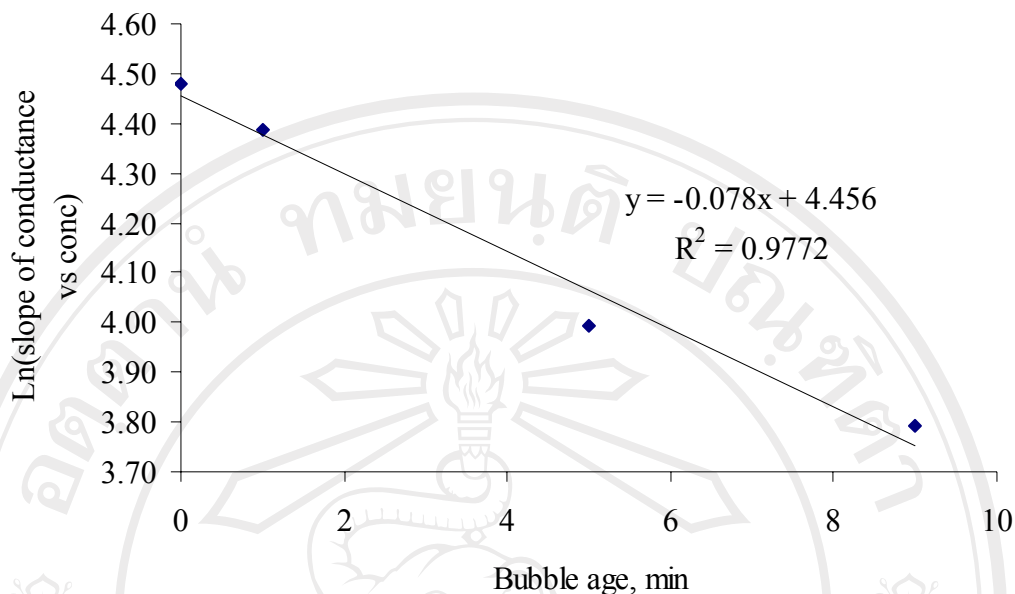
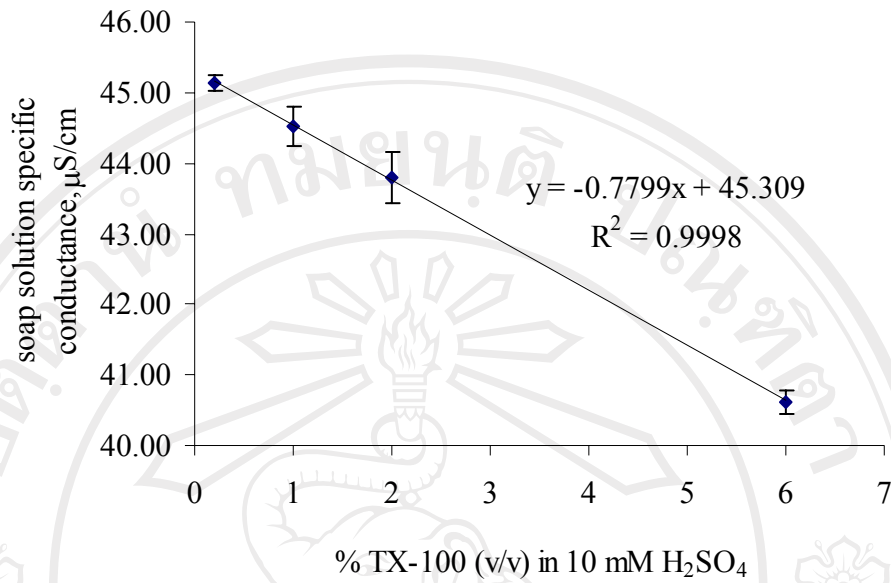


Figure 3.8 Logarithm of the slope values in Figure 3.7 decrease linearly with the bubble age

### 3.2.3 Effect of TX-100 content to conductance

As previously stated, the conductance of a bubble at any specific time is linearly related to the conductance of the soap solution. The conductance of 10 mM  $\text{H}_2\text{SO}_4$  solution, decreases with increasing concentrations of TX-100 (0.2, 1, 2 and 6% v/v, without glycerol) added, in both soap solution and soap bubble as shown in Figure 3.9. The linear  $r^2$  for the relationship in both bubble making solution and soap bubble are 0.9999 and 0.9945, respectively. Increasing the TX-100 content increases the viscosity of solution thus causing a decrease in the conductance.

(a)



(b)

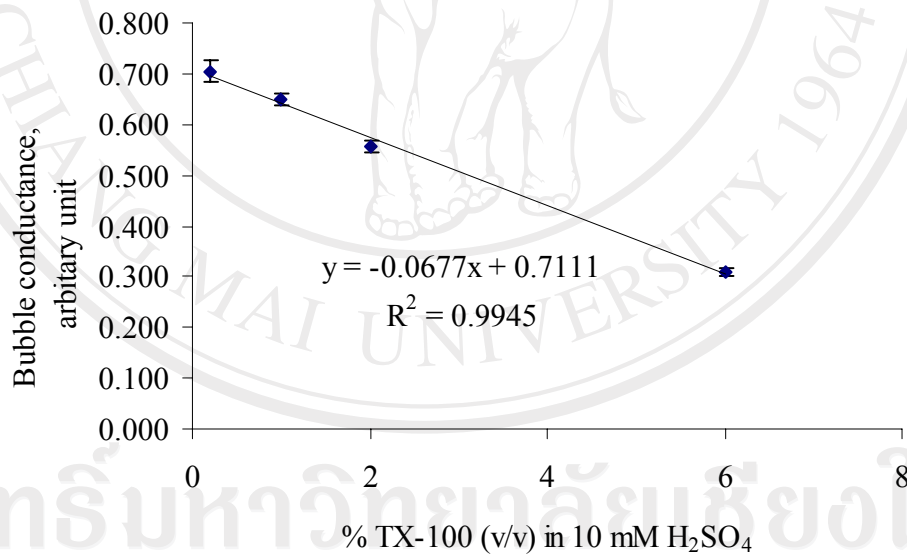


Figure 3.9 Conductance of 10 mM  $\text{H}_2\text{SO}_4$  solution as a function of TX-100 (0.2, 1, 2, 2.0 and 6% v/v) concentration added. a) Specific conductance of bubble making solution, b) bubble conductance. Both specific conductance of solution and bubble conductance linearly decrease with increasing glycerol content

### 3.2.4 Conductance vs. bubble size

These experiments were performed with a bubble making solution containing 10 mM H<sub>2</sub>SO<sub>4</sub> in 2% TX-100 that flowed under gravity from a constant height to the bubblehead as demonstrated in Figure 3.10. The volume of the solution delivered per unit time was calibrated gravimetrically. The total volume of the solution delivered could be adjusted by timing the on/off switching of solenoid valve SV1, however presently a fixed volume was used even though bubble size was varied. The bubble size was varied by changing the on-duration of solenoid valve SV2 which allows air to inflate the bubble. Brass electrodes of diameter 2.7 mm were used in this experiment and the electrode location was varied for the different size of bubbles so that they just touched the bubble. The interelectrode distance was changed from 28.7 to 39.0 mm and the measured bubble size was within  $\pm 0.2$  mm of this.

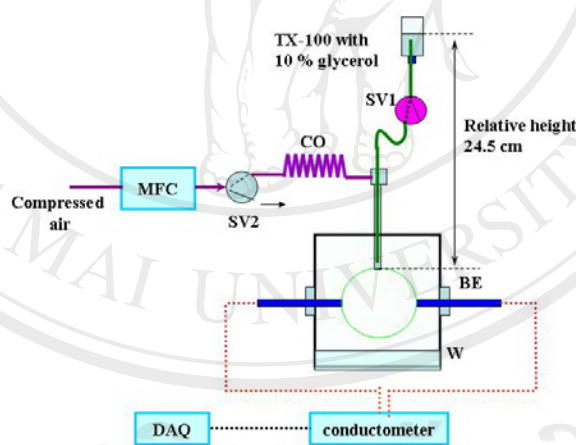


Figure 3.10 Setup for conductance measurement of varying bubble size: soap solution flows by gravity through solenoid valve SV1 to bubblehead and compressed air controlled by mass flow controller, MFC passes through solenoid valve SV2 to inflate bubble. The conductance between brass electrodes BE, 28.7 - 39.0 mm apart, was measured

Figure 3.11 shows the temporal conductance profile for various bubble sizes. At any particular value of  $\tau$ , the bubble conductance decreases with increasing bubble size. This is intuitive for two reasons: first, the interelectrode separation increases and second, at constant bubble liquid content, increased diametric size must mean reduced film thickness.

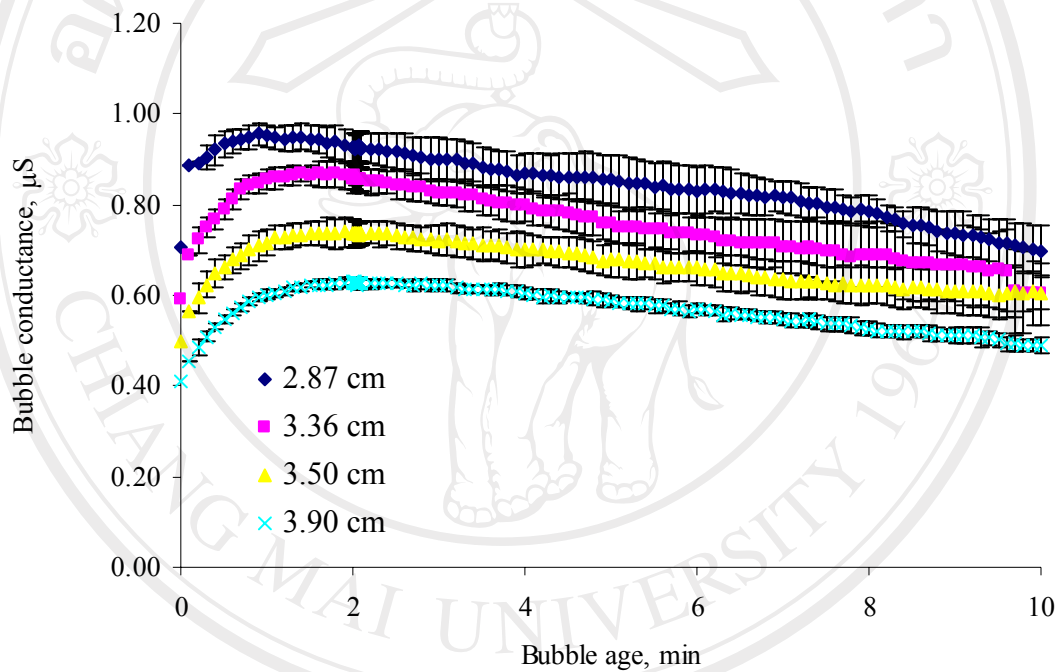


Figure 3.11 Temporal conductances from various bubble sizes

When the film thickness is computed according to equation 3.3, the uncertainties in this geometric calculation primarily arise from uncertainties in the solution volume  $V_s$ . This film thickness can be used to calculate the bubble conductance through equation 3.4 and these computed values can be compared with the experimentally measured values (at  $\tau = 1$  min,  $n = 3$  bubbles). This is shown in Figure 3.12.

The correlation between the calculated and the measured conductance values are excellent except for the smallest size. For the relatively smallest bubble size, the excess liquid in bubble may have rapidly flowed to the bottom rather than be distributed into a film of even thickness as implicitly assumed in equation 3.4.

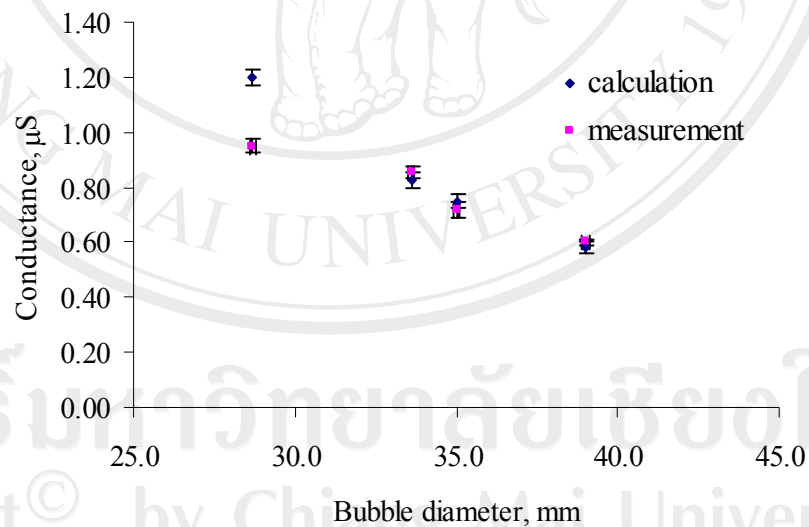


Figure 3.12 Measured bubble conductance for various bubble sizes compared to conductance values computed from known solution specific conductance, geometrically estimated thickness (equation 3.3) measurement and the bubble conductance model (equation 3.4)

### 3.2.5 Film thickness from conductance measurement compared to that from optical measurement

From the known specific conductance  $\sigma$  of the soap solution and the photographically measured bubble radius  $r_b$ , the film thickness  $\delta$  can be calculated by a transposed form of equation 3.4, noted below as equation 3.9:

$$\delta = \frac{G \ln \left( \cot \frac{r_e}{2r_b} \right)}{\pi \sigma} \quad [3.9]$$

This calculated thickness is shown in Figure 3.13 for solutions of 10 mM  $\text{H}_2\text{SO}_4$  in 2% TX-100, 10% glycerol, with and without 2-6% dye. The data are also shown for a solution of 5 mM  $\text{H}_2\text{SO}_4$  in 2% TX-100, 10% glycerol. The film thickness of solutions without dye show greater value for the first minute but decreases more rapidly with time. From Figure 3.13, the film thickness from optical measurement for four different bubble ages are shown as individual points with error bars. In essence, film thicknesses determined from the conductometric and photometric measurements are the same within experimental uncertainty.

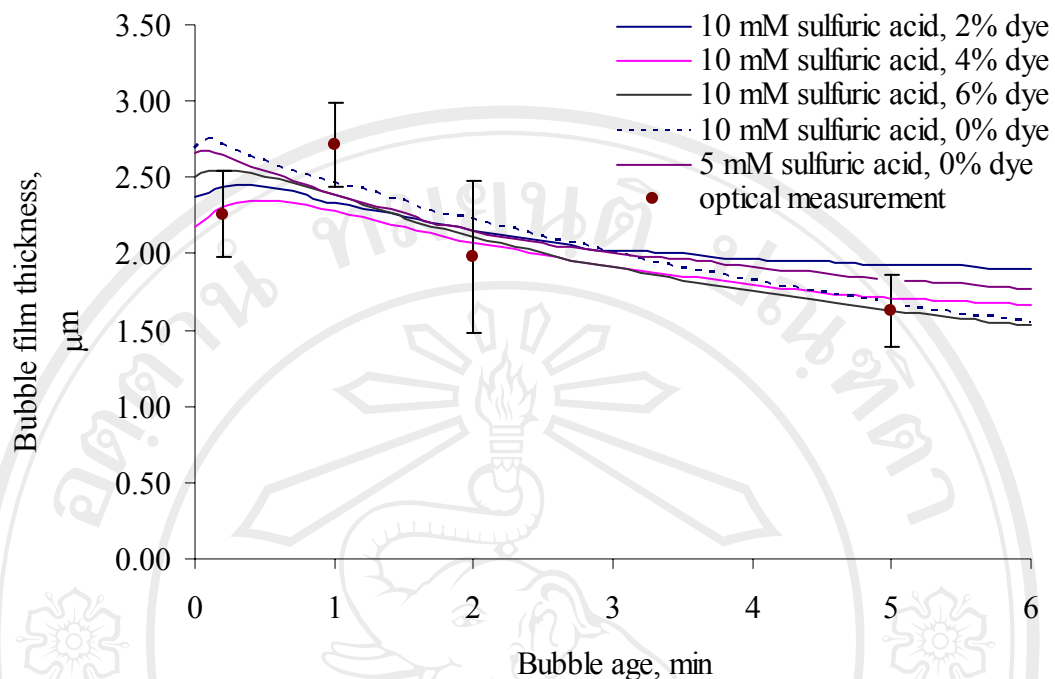


Figure 3.13 Bubble film thicknesses based on bubble conductance: Comparison with optically measured film thickness (n=3)

### 3.2.6 Bubble as conductance flow cell

After the bubble is formed and touches the electrodes, a drain tube was placed at the bottom of the bubble and the bubble was used as a flow-through cell. The setup is shown in Figure 3.14. The output of a syringe pump SP proceeded through a 6-port injection valve IV and then connected to the output of the solenoid pump SVP through a Y-connector. After the bubble is formed with the solenoid pump further bubble making solution was continuously pumped with the syringe pump at the desired flow rate. Sulfuric acid (1 mM, 5 μL) was periodically injected; the results are shown in Figure 3.15.

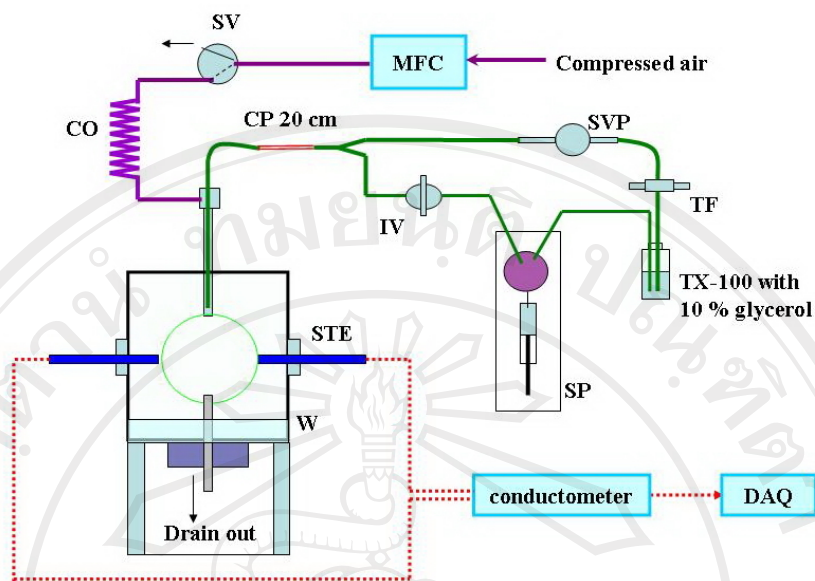


Figure 3.14 Setup of bubble as a conductometric flow cell

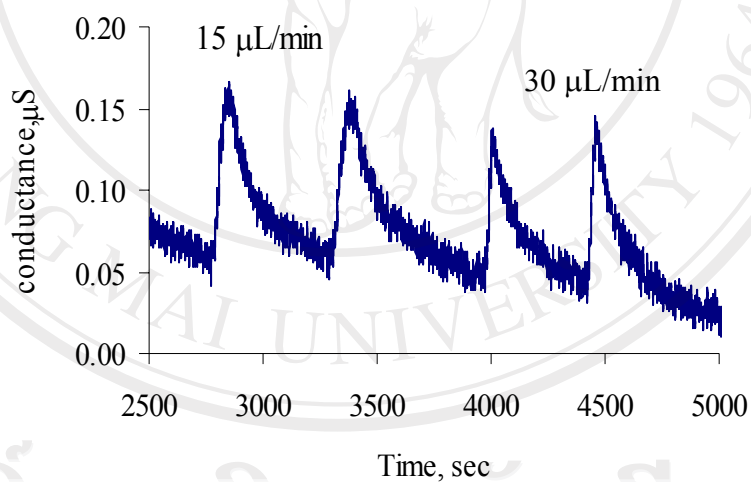


Figure 3.15 FIAgram obtained with bubble flow cell. After making the bubble, soap solution (2% TX-100, 10% glycerol, was continuously pumped at the indicated flow rate by an auxiliary pump and the  $5 \mu\text{L}$  of  $10^{-3} \text{ M}$   $\text{H}_2\text{SO}_4$  in the same soap solution matrix was injected

### 3.3 Soap bubbles for gas sampling and analysis

#### 3.3.1 Application of soap bubble for SO<sub>2</sub> gas sampling and analysis

The application of a soap bubble as efficient (rapid and significant preconcentration) gas sampling interface was demonstrated through analysis of SO<sub>2</sub> gas. Hydrogen peroxide in solution has often been used for the determination of SO<sub>2</sub> gas by oxidizing it to sulfate and measuring the resulting sulfate ion. Examples of this concept include ion chromatographic [111] or nephelometric [112] sulfate determinations.

Sulfur dioxide gas of known concentration from a Henry's law-based generation source, (cf. Chapter II) was diluted to the desired concentration by using secondary dilution air stream at flow rates of 200-2000 sccm that was first humidified by passing through two sequential bubblers. The diluted standard was allowed in part to vent through a soda-lime packed tube and 350 sccm was introduced at the top of the chamber containing the bubble as shown in Figure 3.16. The flow splitting was achieved with the help of two polypropylene flow control valves.

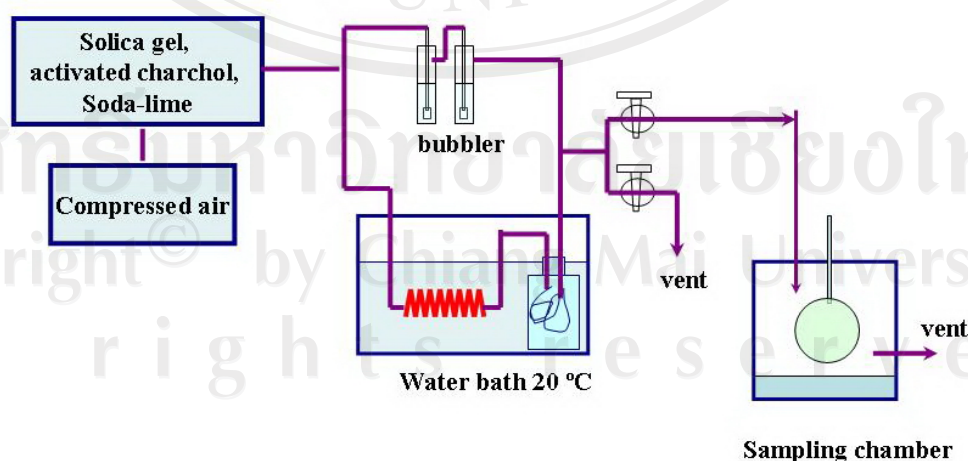


Figure 3.16 Testing bubble-based collection/analysis system with diluted SO<sub>2</sub> standards

The oxidation reaction of  $\text{SO}_2$  gas in liquid was studied by Schwartz and Freiberg [113]. The uptake of  $\text{SO}_2$  by a bubble containing  $\text{H}_2\text{O}_2$  is similar to uptake by a cloud droplet containing  $\text{H}_2\text{O}_2$  in which was studied by Schwartz and Freiberg. In bubbles, uptake of  $\text{SO}_2$  is composed of 5 steps; (i) transport of the gas to the gas-liquid interface; (ii) Henry's law dissolution at the interface; (iii) ionization of dissolved  $\text{SO}_2$  to  $\text{HSO}_3^-$  and  $\text{SO}_3^{2-}$ ; (iv) oxidation of the S(IV) anions by  $\text{H}_2\text{O}_2$ ; and (v) mass transport of the  $\text{H}_2\text{SO}_4$  to the interior whole liquid. Steps (ii) and (iii) are not expected to be rate limiting, and with large amounts of  $\text{H}_2\text{O}_2$  as used here, step iv is also going to be rapid. In the present experimental setup (experimental condition are given in Table 3.1), the test gas is introduced from the top. As a result, the top half of the bubble captures the analyte efficiently as the gas is first introduced. Gas-phase diffusion becomes the limiting factor for the bottom half of the bubble. (This limitation can be overcome by introducing the gas at multiple points around the bubble; however, this was not presently attempted.) On the other hand, when one measures the conductivity of the bubble as a whole, the distribution of the  $\text{H}_2\text{SO}_4$  formed in the bubble becomes the rate-limiting process because in a series circuit the highest resistive element controls the overall passage of current. This is quite similar to the case of a cloud droplet where typically the slowest step is diffusion of  $\text{H}_2\text{SO}_4$  within the bulk liquid.

The temporal conductance profile with 1200 ppbv  $\text{SO}_2$  sampled at 200 mL/min is not linear as shown in Figure 3.17 while the a profile from a higher gas sampling rate, such as 300 mL/min (with either 240 or 720 ppbv  $\text{SO}_2$ ), shows a more linear relationship. The sample gas flow circulates the bubble film liquid due to frictional drag, inducing convective mixing that is a strong function of the precise gas

flow rate. These data suggest that the diffusion and redistribution of sulfuric acid within whole liquid in bubble is limiting step and is quite similar to the case of a cloud droplet where typically the slowest step is diffusion of  $\text{H}_2\text{SO}_4$  within the bulk liquid [114].

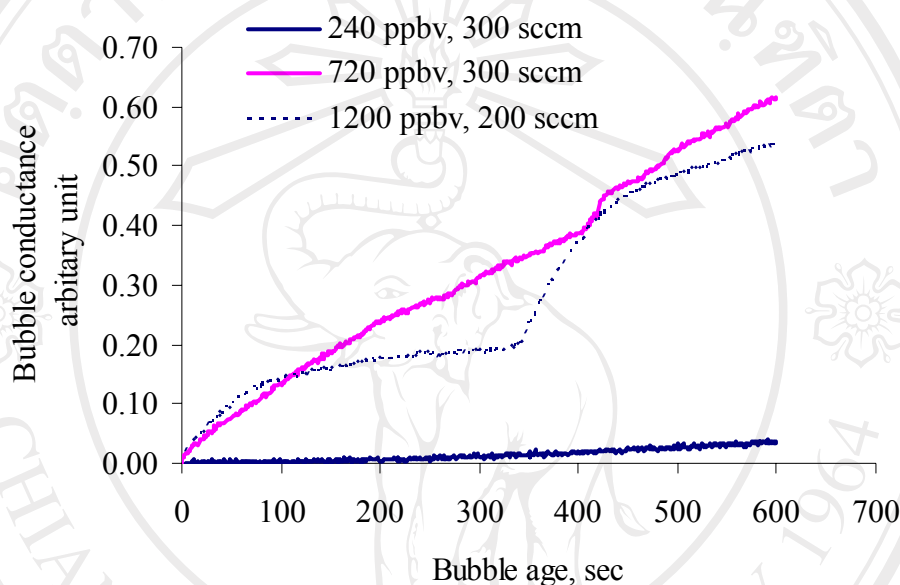


Figure 3.17 Temporal bubble conductance profiles from various  $\text{SO}_2$  sampling rates; 1200 ppbv at 200 mL/min shows a non-linear increase of conductance with time, while a sampling rate of 300 mL/min produces a nearly linear increase at two different concentrations

In this experiment,  $\text{SO}_2$  was sampled without electrode washing system. Without washing the electrodes between runs, there is some carryover effect from residual  $\text{H}_2\text{SO}_4$  that stays on the electrodes as a product of previous  $\text{SO}_2$  sampling (product of  $\text{SO}_2$  and  $\text{H}_2\text{O}_2$ ). In addition, there is also residual  $\text{SO}_2$  left in the chamber. As shown in Figure 3.18, an additional humidified pure air line flowing at a rate of

350 sccm through SV1 was used to flush the bubble chamber for 120 s (0-120 s) to flush remaining SO<sub>2</sub> in chamber. This flow also efficiently removes most of the previous soap solution from the electrode surface. For each run, the beginning bubble conductance was reset as zero, to constitute the new baseline before sampling with SO<sub>2</sub>. The bubble conductance at 120 s was subtracted from the final bubble conductance at 600 s and the net increase in conductance is plotted against the SO<sub>2</sub> concentration as shown in the upper plot of Figure 3.19. The graph shows 2 of linear calibration ranges. The first linear  $r^2$  of calibration plot is 0.9778 while the second range is 0.9933. The detection limit calculated from first liner calibration range is 37 ppbv. With humidified zero air flush between samples, the reproducibility was 3.9 % in relative standard deviation (n=5).

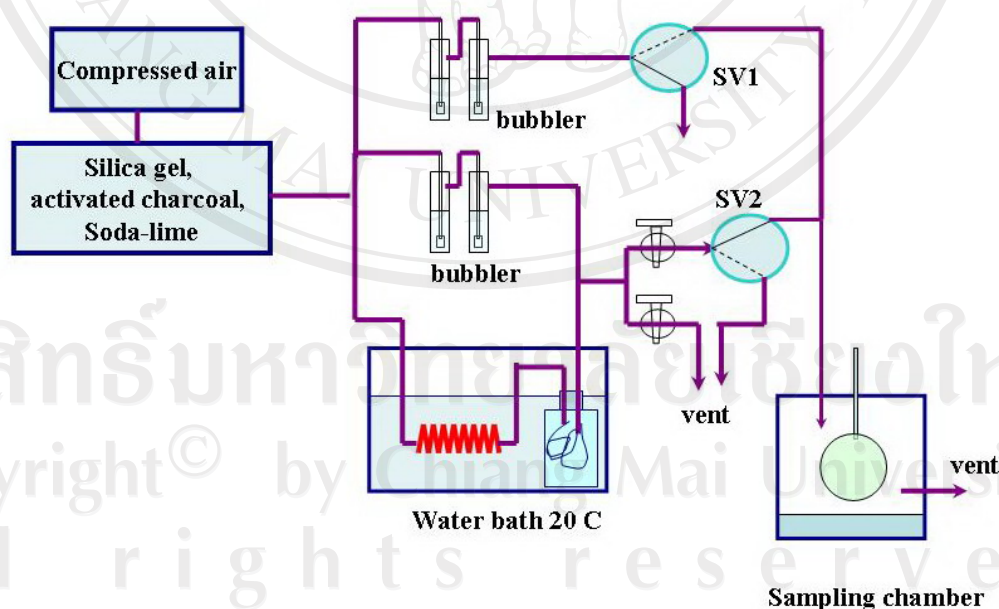


Figure 3.18 Arrangement for SO<sub>2</sub> sampling with provision for flushing chamber with clean humidified air between samples

Table 3.1 Experimental condition for SO<sub>2</sub> sampling with a soap bubble

<b>Experimental parameter</b>	<b>Value</b>
Soap solution	Purified 2% Triton X-100
Soap solution volume , $\mu\text{L}$	5 (1 actuation)
Bubble inflation air flow rate, sccm	180
Bubble inflation time, s	5
Gas sampling time, min	10
Pre-sampling time, min	2
Sample gas flow rate, mL/min	350

ลิขสิทธิ์มหาวิทยาลัยเชียงใหม่  
 Copyright© by Chiang Mai University  
 All rights reserved

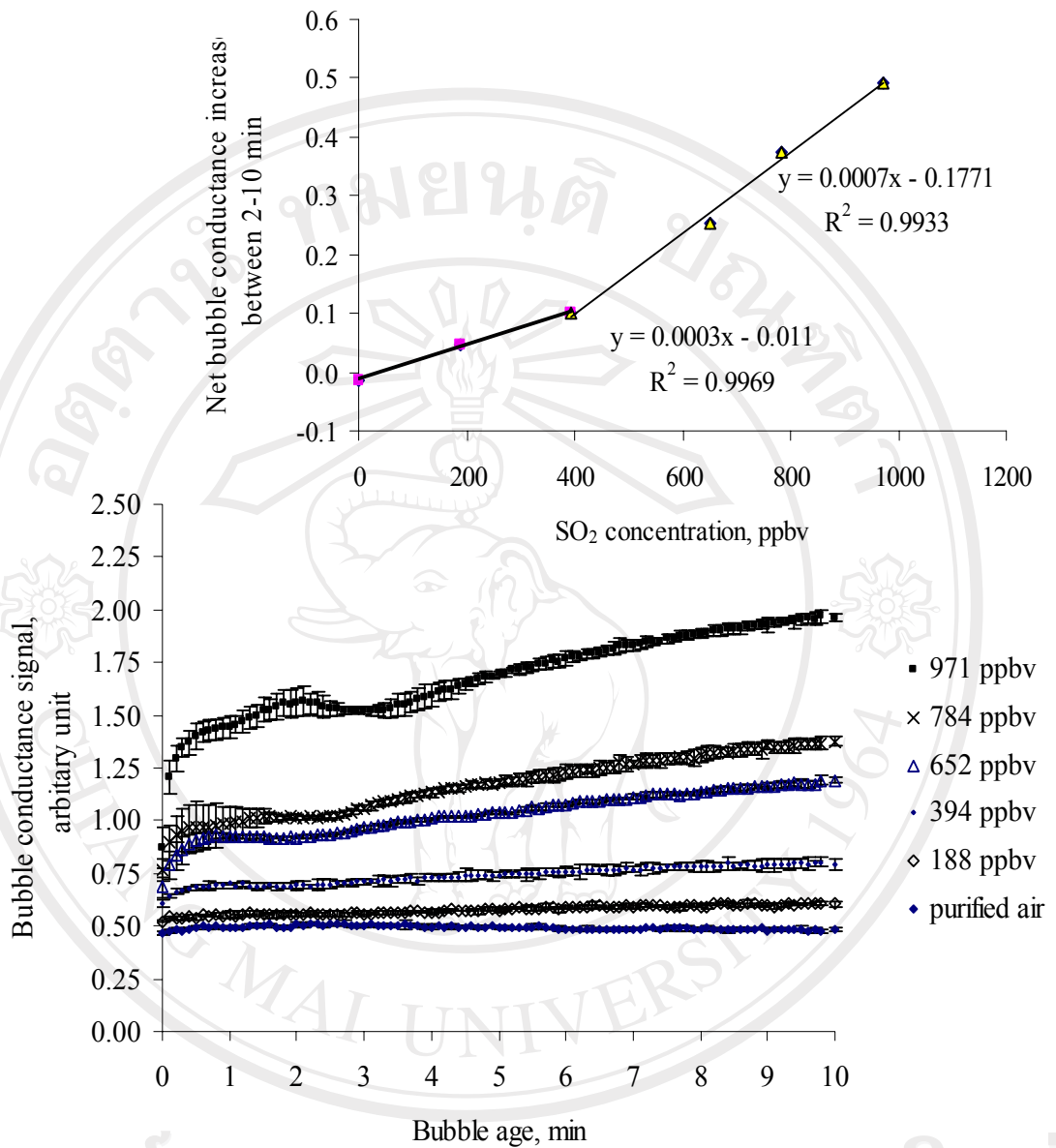


Figure 3.19 Top: Net bubble conductance increase between  $\tau = 2$  min and  $\tau = 10$  min plotted against SO<sub>2</sub> concentration sampled. Bottom: temporal profile of bubble conductance as a function of SO<sub>2</sub> concentration sampled

At gas sampling rates of  $\geq 350$  ml/min, the conductance linearly increases with time regardless of  $\text{SO}_2$  concentration, it is therefore possible to use a short sampling period. For a 30 s sampling time, the linear calibration equation is:

$$\text{Signal, volts} = 2.77\text{E}^{-4}[\text{SO}_2, \text{ppbv}] - 2.73\text{E}^{-2} \quad [3.10]$$

As shown in Figure 3.20. Problems from  $\text{H}_2\text{SO}_4$  accumulation is expected to be less than that from longer sampling times. Bubble-based sampling and analysis devices can thus be applied for near real time  $\text{SO}_2$  measurement.

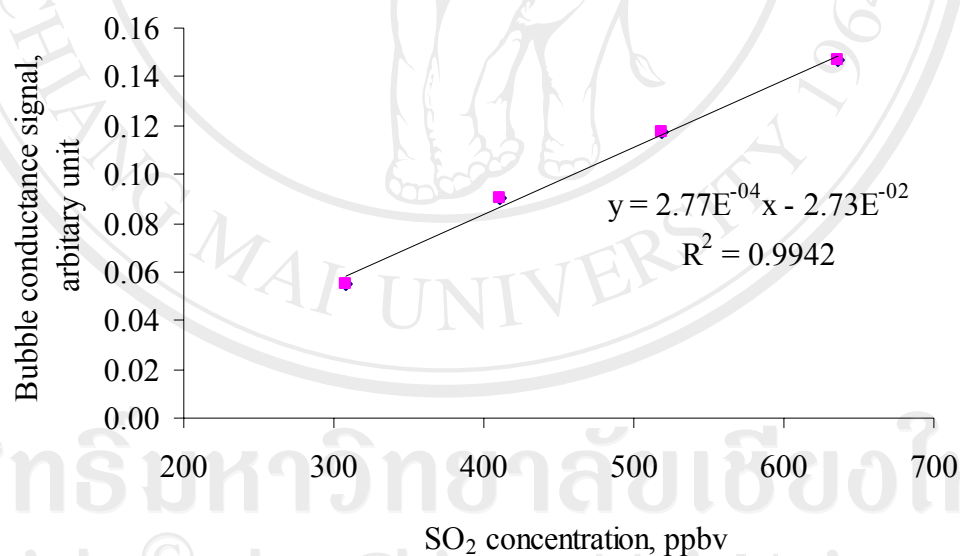


Figure 3.20 Conductance signal vs.  $\text{SO}_2$  concentration for 30 s sampling

### 3.3.2 Automation for soap bubble gas sampling and analysis by using SIA

A bubble making system using sequential injection analysis (SIA) was assessed. It can be operated and controlled automatically with in-house developed programming. The bubble head, SI system, and SI protocol are depicted in Figure 3.21 and 3.22, respectively. The syringe pump and selector valve were used for liquid manipulations. The bubblehead was made from a 3-way connector. The program sequence and experimental conditions for making soap bubble are shown in Table 3.2 and Table 3.3, respectively. The electrodes are platinum wires attached from the top of the chamber; they were 2.1 cm apart. The electrodes touch the bubble film when the bubble is inflated as shown in Figure 3.22. The presence of a finite conductance indicates the bubble-electrode contact and thus this can be used to stop further inflation under active control. The syringe pump aspirates 1000  $\mu\text{L}$  of 2% TX-100 to holding coil HC1 and dispenses to holding coil HC2 which has volume of 750  $\mu\text{L}$ . As a result, some excess 2% TX-100 ( $\sim$  about 250  $\mu\text{L}$ ) was dispensed and flows out to waste through the bubblehead. Then the water was aspirated to HC1 and the desired volume of 2% TX-100 was dispensed from HC2 to the bubblehead by the dispensed water. Solenoid valve SV was turned on to let air flow (controlled and monitored by rotameter RT) to inflate the bubble. The bubble conductance was measured with the platinum wire electrodes. Following the measurement, water was dispensed through port 1 and 4 of the selection valve to wash both electrodes and as a result the bubble was removed from the electrode.

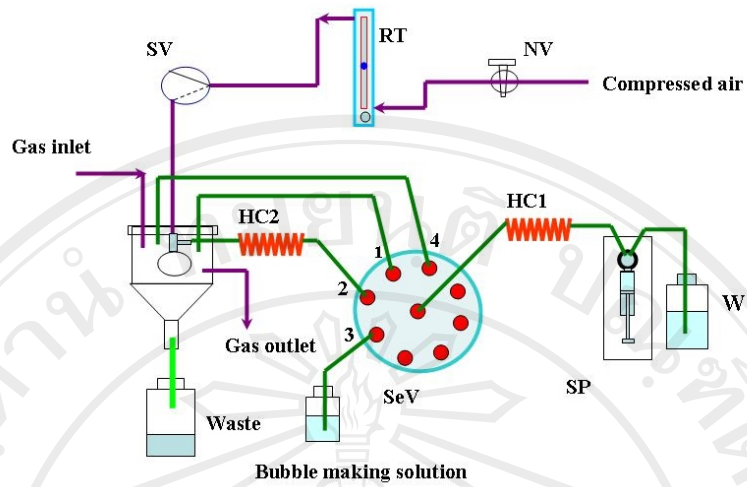


Figure 3.21 Sequential fluid delivery system to make bubble and wash electrodes

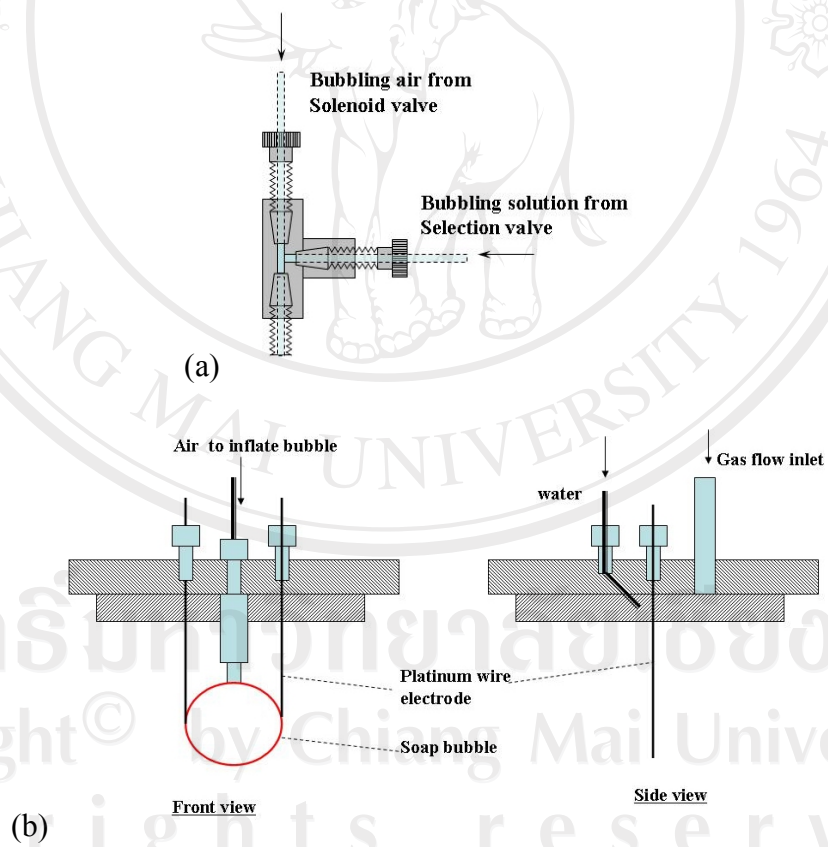


Figure 3.22 Bubblehead and electrode arrangement to make bubbles in a sequential fluid handling system: a) Bubblehead, b) electrodes and electrode-washing system

Table 3.2 Protocol for making bubbles with sequential fluid handling system

Step	Valve position*	Comment
1	3	Aspirate soap solution (TX-100)
2	2	Dispense soap solution to rinse holding coil HC1 and bubblehead
3	3	Aspirate 1000 $\mu$ L soap solution
4	2	Dispense 1000 $\mu$ L soap solution to holding coil HC2
5	2	Aspirate 1000 $\mu$ L water from reservoir
6		Start bubble making process
6.1	2	Dispense soap solution in HC2 to bubble head
6.2	2	Turn on solenoid valve to inflate the bubble
6.3	2	Turn off solenoid valve when bubble contacts the electrodes
6.4	1	Dispense 500 $\mu$ L water to HC1
6.5	4	Dispense 500 $\mu$ L water from HC1 to wash electrodes.
6.6		Aspirate water from reservoir- prepare for formation of next bubble

\*refer to Figure 3.21

Although, the exact contact area of the platinum wire electrodes were not controlled in the present experiments, the reproducibility bubble conductance for identically made bubbles ranged from 3-5 % rsd. The correspondence of bubble conductance made with soap solutions containing  $1 \times 10^{-5}$  M to  $1 \times 10^{-2}$  M  $H_2SO_4$  with the conductance of the soap solutions are shown in Figure 3.23.

Table 3.3 Experimental conditions for making soap bubbles by the sequential fluid handling system

Experimental parameter	Value
Soap solution	purified 2% TX-100
Soap solution volume <sup>*</sup> , $\mu\text{L}$	15
Inflation air flow rate <sup>**</sup> , mL/min	140
Inflation time <sup>***</sup> , s	10
Conductance measurement time, s	60

\*delivery by using syringe pump in SI system

\*\* controlled by using needle valve, flow rate measured by using calibrated rotameter

\*\*\* The time of turn on/off solenoid valve to let air flow to bubble head

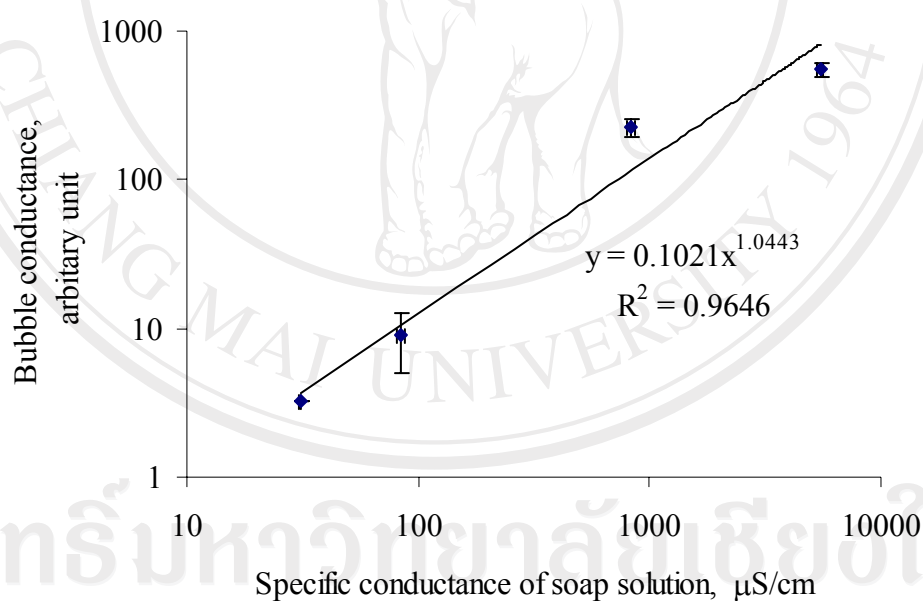


Figure 3.23 Correspondence of specific conductance of bubble making solution vs. bubble conductance, bubble made by the sequential fluid handling system

### **3.4 A planar soap film as a membrane**

A planar soap film can be considered as a liquid membrane and was investigated for selective transport of analytes in the vapor phase. A donor stream bearing the compound(s) of interest flows on one side of the film and the other side is examined for the amount of the transported material. Obviously, the film must have good stability. The life time of a planar soap film, made as described in the experimental section, was investigated under various conditions.

#### **3.4.1 Effect of vertical vs. horizontal film placement**

In these preliminary experiments, effect of placement of the planar soap film as vertical and horizontal plane on life time of the film was investigated. The plastic caskets were modified to attach a rectangular perspex ledge in both horizontal and vertical placements in a box which has water at the bottom as depicted in Figure 3.24 and 3.25. The dimensions of opened window of plastic ledge (for attachment of bubble film) are 7.5x 4.5 cm and 6.0x 4.5 cm for horizontal and vertical placements, respectively. The soap film was made by sliding soap soaked plastic sheet on such ledge (in the same way as explained in experimental section). The life time of soap films of both placements without flowing of air were compared.

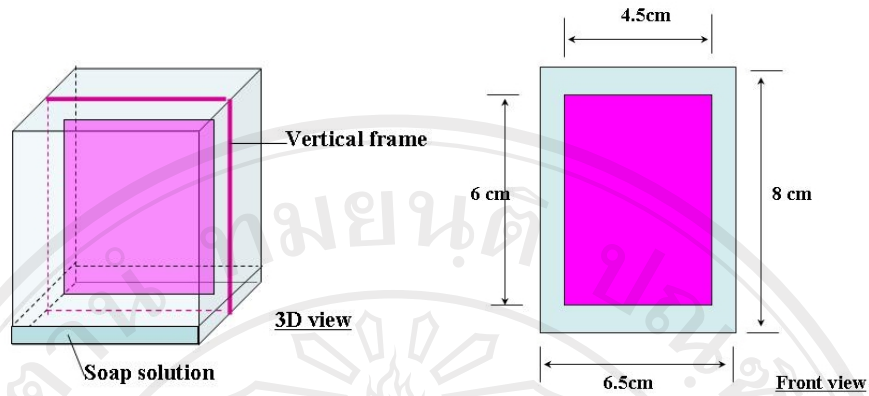


Figure 3.24 Schematic diagram of vertical placement of plastic ledge in a box

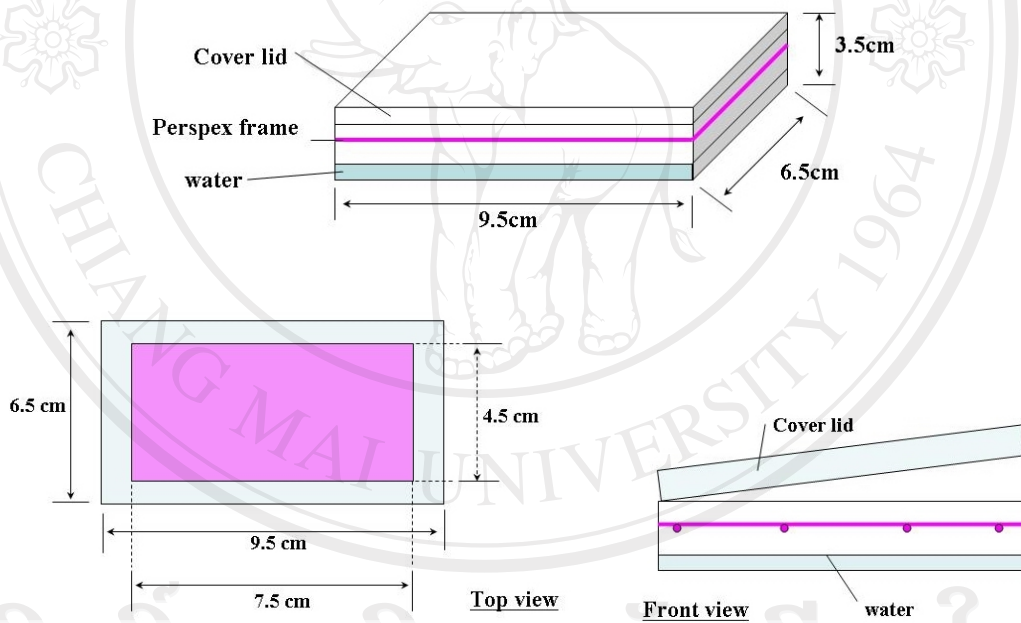


Figure 3.25 Schematic diagram of horizontal placement perspex ledge in box. a) 3D, b) top view, c) front view

It was found that the life time of a horizontally placed film was much longer than a vertical placement (39-90 s compared to 7-30 s, respectively,  $n=10$  in each case). It can be readily observed in a vertically placed film that the solution in the film moves down to the bottom and cause the upper part of the film to gradually thin out and thus rupture. Hence, we chose a horizontally placed soap film for further studies.

#### **3.4.2 Planar soap film: variation in glycerol contents**

The stability of horizontal soap films with various glycerol contents was investigated without air flowing. The soap film life time consistently increased with increasing glycerol content as shown in Table 3.4 ( $n=10$  in each case).

For soap films containing 30 % glycerol, life times were consistently longer than 720 s (12 min). However, high glycerol content reduces the transport flux (see section 3.5.3). For our permeation experiments, a film lifetime of 5 min was long enough. Therefore, the 10 % glycerol (v/v) in 5%TX-100 was selected for further experiment.

Table 3.4 Horizontal film lifetime containing various amounts of glycerol (n = 10, in each case)

Soap solution		Life time(s)	
% TX-100	% glycerol (v/v)	Minimum	Maximum
2	0 %	6	144
5	0 %	25	180
5	10%	120	>300
5	20%	420	>600
5	30%	>720	>720

### 3.4.3 Planar soap film lifetime under varying gas flow conditions

The investigation of soap film stability under flow conditions was carried out using the set up described in Chapter II. Pure air was used in both chambers. Effects of choice of the chambers (donor vs. receiver), inlet flow rate was investigated.

The identity of the donor vs. receiver chamber (top vs. bottom) affects life time of soap film as shown in Table 3.5. In these experiments the receiver chamber was always at atmospheric pressure while the flow in the donor chamber created a positive pressure there relative to the receiver chamber. As a result, the film always bulges from the donor to the receiver side. Making the receiver side the bottom, would cause the soap solution to flow down and accumulate at the bottom of film as demonstrates in Figure 3.26: causing added gravitational stress. As a result, the soap film has a more limited life time than when the receiver side is the top. With the receiver chamber at the top, excess soap solution flows from the film to the edge, providing a longer life time. This configuration was henceforth chosen.

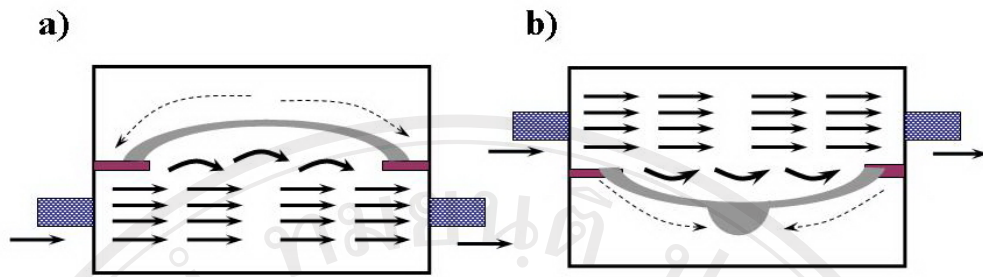


Figure 3.26 Effect of chamber identities: a) Receiver chamber at top, film bulges upward and excess solution flows to soap film edge b) Donor chamber at top, film bulges downward, excess solution flows to film bottom and accumulates as a drop

Table 3.5 shows film life time under various conditions of flow and identity of the donor chamber. For  $\leq 100$  mL/min flow the film life time is longer than 10 min. The life time of soap film with 100 mL/min air flow rate and flow in the lower part of the permeation chamber is long enough for vapor permeation study.

Table 3.5 Life time of 5% TX-100 + 10% glycerol soap film under various flow conditions

Donor chamber flow rate (mL/min)	Life time of soap film, s							
	Donor chamber on top				Receiver chamber on top			
	average $\pm$ sd		min-max		Average $\pm$ sd		min-max	
0	> 600 (n=7)							
100	351 $\pm$ 179	(n=9)	240	>600	> 480	(n=9)	>420	>600
200	122 $\pm$ 50	(n=10)	80	420	219 $\pm$ 105	(n=7)	80	238
300	43 $\pm$ 81	(n=3)	10	265	155 $\pm$ 65	(n=9)	96	230

### 3.5 Permeation through soap film

The transport of  $\alpha$ -pinene, through the soap film was investigated in both (+) and (-) forms. The  $\alpha$ -pinene (+) and (-) vapors were generated by using a diffusion source and measured by sampling with solid phase micro extraction (SPME) followed by gas chromatographic analysis on a chiral column.

#### 3.5.1 Investigation on SPME-GC determination of $\alpha$ -pinene

The  $\alpha$ -pinene vapor was sampled with SPME (PDMS-100  $\mu$ m, Supelco) and determined for its concentration by a gas chromatograph using an operating condition as explained in experimental section. Firstly, in order to confirm retention time of both chiral forms, the SPME fiber was placing in the headspace of the plus (+) or minus (-) liquid of  $\alpha$ - pinene standard (product from Fluka) for 1 s. The retention time of (-) and (+)  $\alpha$ - pinene is about **14.3** and **14.6** min, respectively, as shown in chromatogram in Figure 3.27.

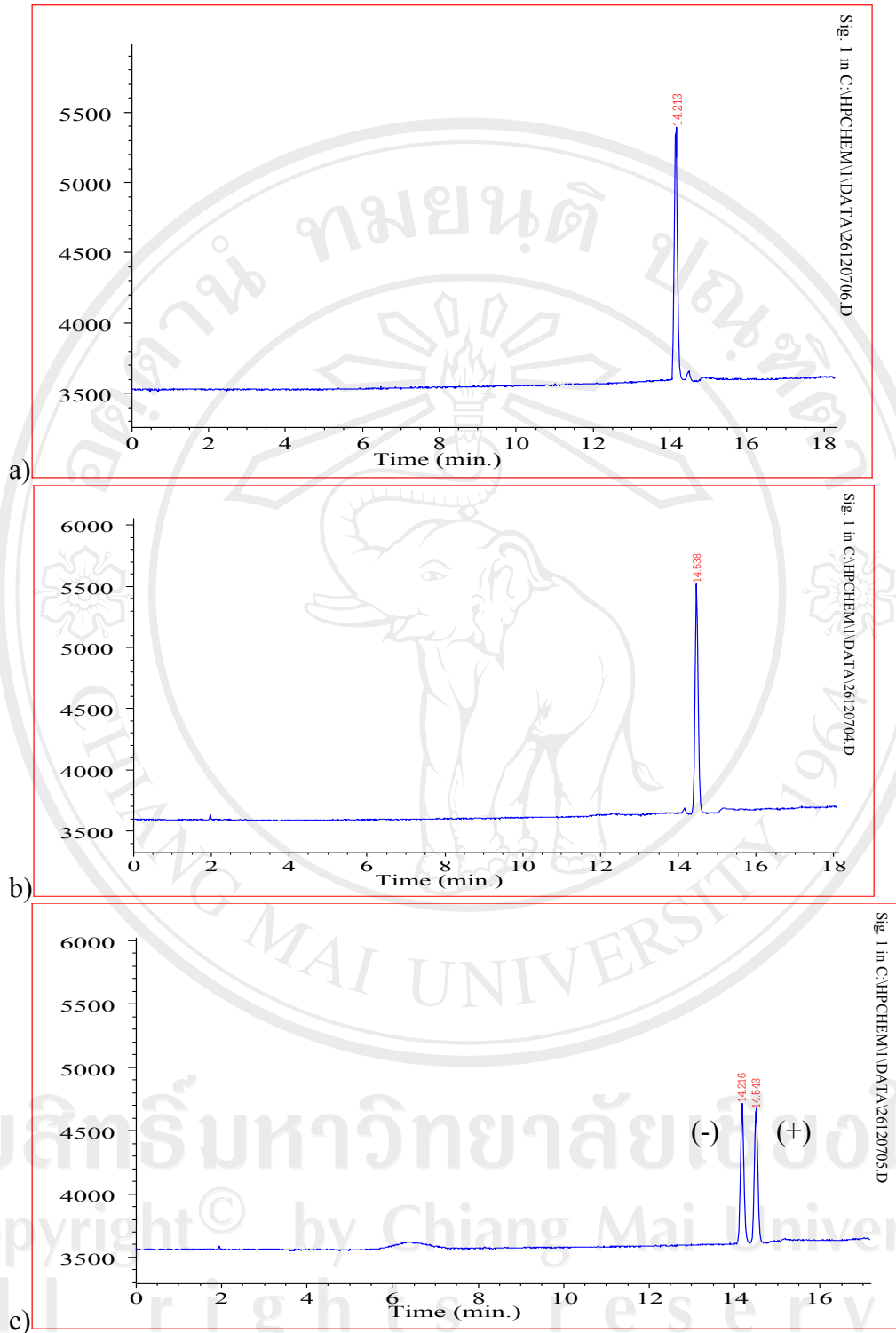


Figure 3.27 Chromatograms of  $\alpha$ -pinene a) minus (-) form b) plus (+) form c) mixed chiral vapors

Validation of quantitative analysis of  $\alpha$ - pinene vapor by using SPME-GC method has been carried out by using known concentrations of  $\alpha$ - pinene ( $1.83 \times 10^{-7}$  g/mL and  $1.76 \times 10^{-7}$  g/mL for plus (+) and minus (-) forms  $\alpha$ -pinene, respectively ) and under the same sampling and analysis condition as explained in experimental section.

Effect of sampling time on peak area obtained from GC for SPME sampling was investigated. Although, sampling time significantly affected to peak area as shown in Figure 3.28, a variation from error in sampling time is about 3 % (error in sampling time 1 s; peak area change of about  $\sim 200$  from peak area 6,000;  $=200 \times 100 / 6000 = 3.3 \%$ ). A sampling time of 30 s was selected for further experiments.

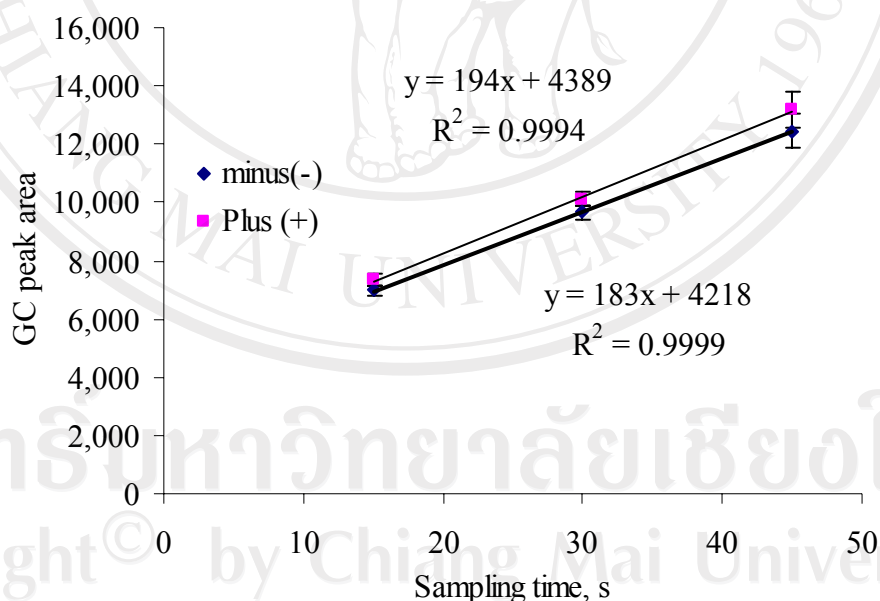


Figure 3.28 Relationship of sampling time and GC peak area of both forms of  $\alpha$ -pinene

The linear relationship of  $\alpha$ -pinene concentration and SPME-GC signal (peak area) as calibration graphs for minus (-) and plus (+) forms, was shown in Figure 3.29 and the equations are given below:

$$A_- = 75.4 * [\text{pinene}(-), \text{ng / ml}] + 133, r^2 = 0.9998 \quad [3.11]$$

$$A_+ = 81.2 * [\text{pinene}(+), \text{ng / ml}] + 128, r^2 = 0.9998 \quad [3.12]$$

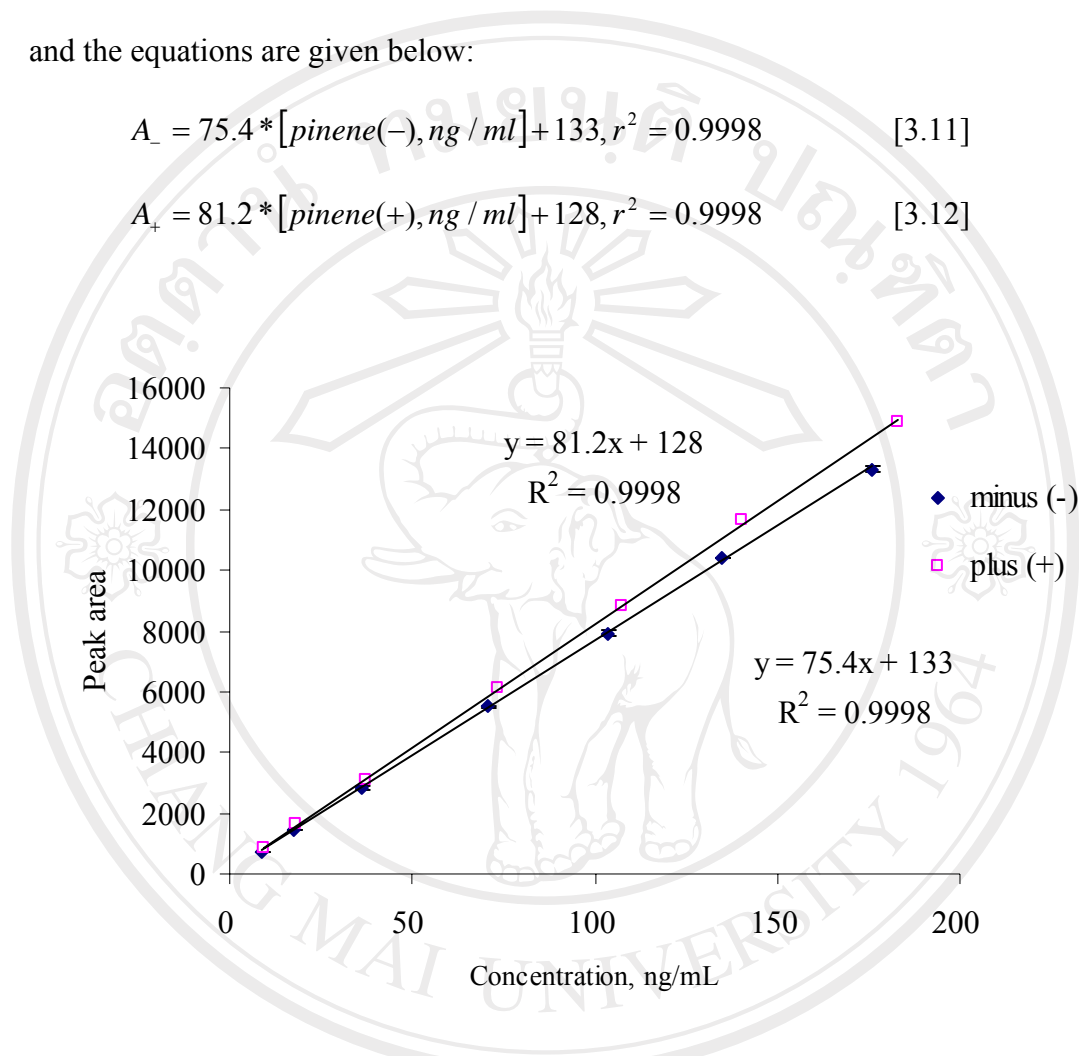


Figure 3.29 Calibration graphs for minus (-) and plus (+) forms of  $\alpha$ -pinene

Inter day variation of SPME-GC signal was evaluated by comparing data on sampling of  $\alpha$ -pinene vapor in U-tube obtained from different experiments carrying out at different days, as summarized in Table 3.6. The whole variation of 5.3%rsd and 2.4 % rsd for minus (-) and plus (+)  $\alpha$ -pinene, respectively was found.

Table 3.6 Peak area, standard deviation and % rsd of SPME-GC determination of (-) and (+)  $\alpha$ -pinene obtained from many days of experiments

Exp* date	Experiment	Peak area					
		minus (-), tr** =14.31			plus(+), tr =14.6		
		Average	sd.	%rsd	Average	sd.	%rsd
1	5% TX-100	14450	239	1.65	15015	257	1.71
1	5% TX-100+ 1-3% CD	14493	3	0.02	15055	20	0.13
2	SPME-GC calibration	13315	107	0.81	14866	136	0.91
3	0.05, 0.5 % TX-100	13498	42	0.31	14358	426	2.97
4	0.05, 0.5 % TX-100	13796	356	2.58	14914	329	2.20
5	0.05% TX-100 + 5-10% CD	13126	520	3.96	15108	621	4.11
5	0.05% TX-100 + 5-10% CD	12512	66	0.53	14503	13	0.09
6	0.05% TX-100 without glycerol	12718	24	0.19	14127	98	0.69
6	0.05% TX-100 with 1 and 5 min flow	12925	120	0.93	14518	235	1.62
<b>Average</b>		<b>13426</b>			<b>14718</b>		
<b>Standard deviation</b>		<b>709</b>			<b>350</b>		
<b>%rsd</b>		<b>5.3</b>			<b>2.4</b>		

\* Exp date= experimental date

\*\* tr= retention time

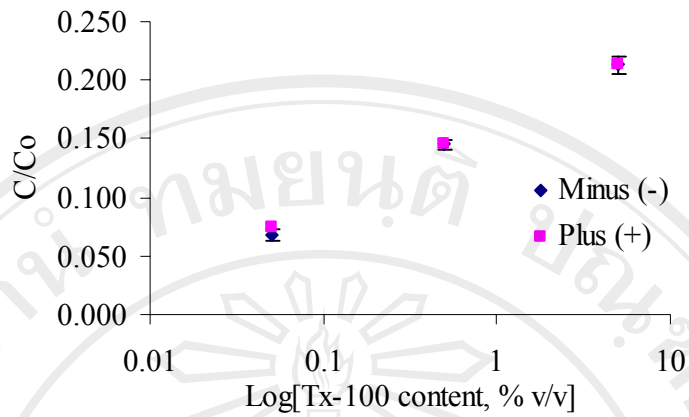
### 3.5.2 Effect of TX-100 content on transport flux

All experiments were conducted with a TX-100 concentration above its critical micelle concentration of 0.2 mM. The lowest concentration used was 0.05% v/v, corresponding to 0.83 mM (density of pure TX-100 is 1.07g/mL and its molecular weight is 647). Up to a concentration of 5% v/v TX-100 was tested.

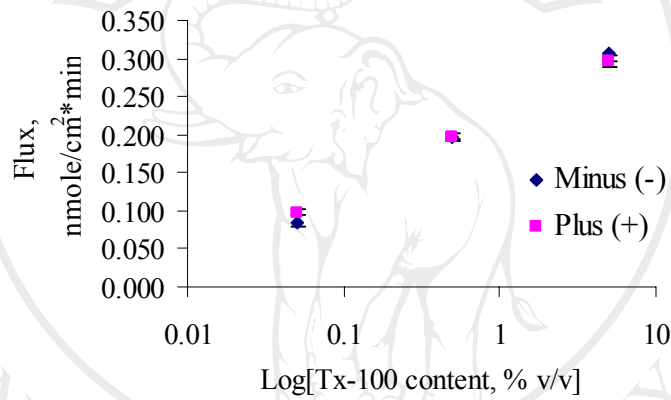
Let  $C_0$  and  $C$ , respectively be the input concentration of  $\alpha$ -pinene fed to the device and the permeate concentration. Increasing TX-100 content of the film consistently provided higher  $C/C_0$ , as well as higher mass flux as shown in Figure 3.30. This may be due to the micelle play a role in transportation of the compounds, similar to those found by Sylvie Cohen-Addad [97]. The higher TX-100 content, the higher the concentration of the micelle available for  $\alpha$ -pinene to be dissolved in. Therefore, the possibility of  $\alpha$ -pinene in soap solution is increased. As a result, permeation flux through soap film increases with increasing TX-100 content.

However, the transport rate for the two forms of  $\alpha$ -pinene through a TX-100 film contents were identical. Both chiral forms transfer across the film at the same rate, resulting in a separation factor of 1 as shown in Figure 3.30.

(a)



(b)



(c)

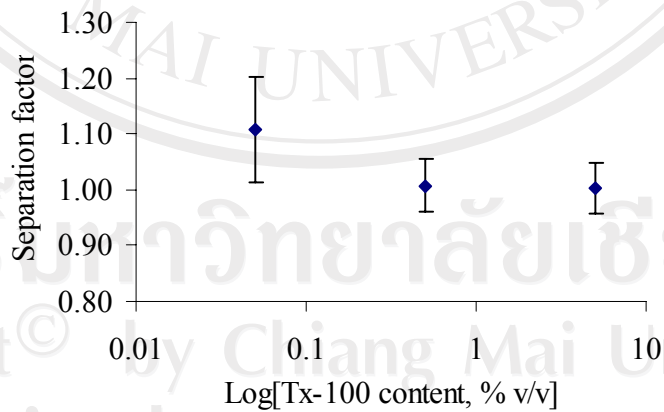


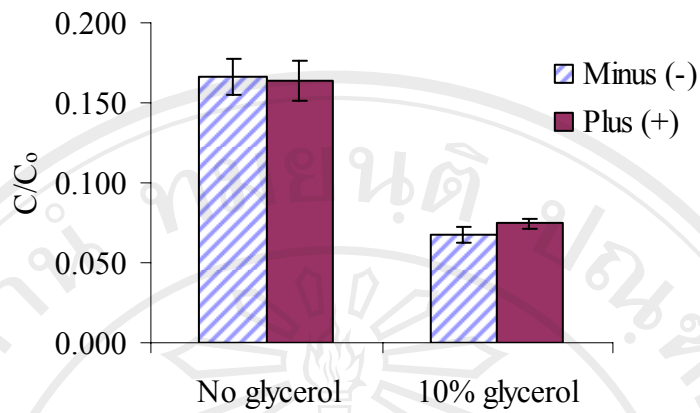
Figure 3.30 Effect of TX-100 content (0.05, 0.5, and 5 % v/v) on  $\alpha$ -pinene transport:

a)  $C/C_0$ , b) transfer flux, c) separation factor

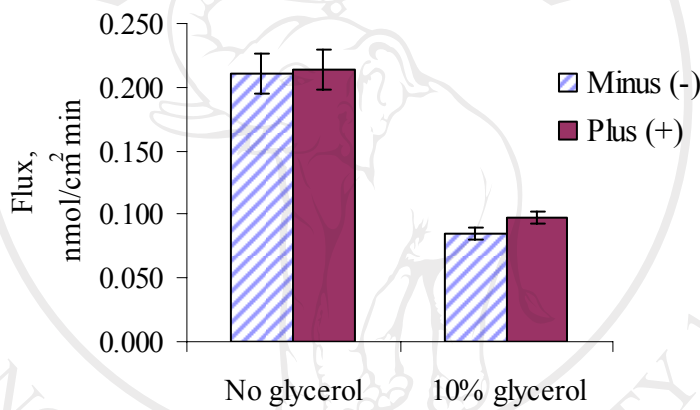
### 3.5.3 Effect of film glycerol content on transport flux

The transport data with and without glycerol in 0.05% TX-100 soap solutions is depicted in Figure 3.31. Incorporation of glycerol in the film uniformly reduced  $C/C_0$  and the total transfer flux. There may be two reasons for this: The solubility of  $\alpha$ -pinene in glycerol will be more limited than in a TX-100 micelle and the presence of the alcohol will inhibit micelle formation. Second, the presence of glycerol may make the film thicker. The presence of glycerol in the film, however, had no effect on the separation factor.

(a)



(b)



(c)

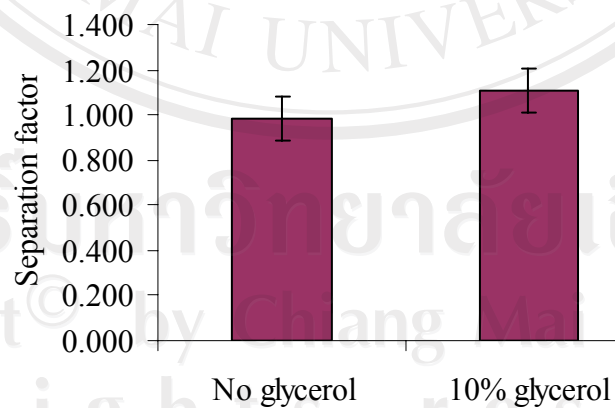


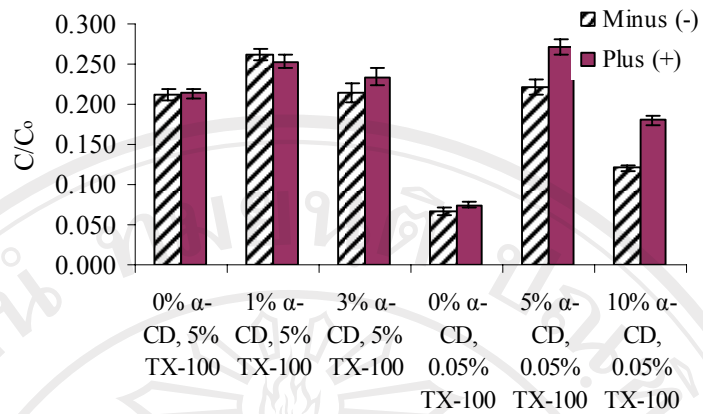
Figure 3.31 Effect of glycerol content on a)  $C/C_0$ , b) transfer flux, c) separation factor

### 3.5.4 Effect of $\alpha$ -cyclodextrin in soap film to $\alpha$ - pinene permeation

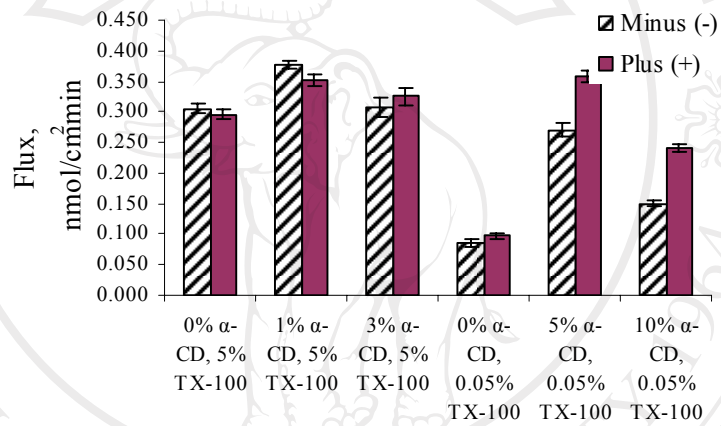
Although solubility of  $\alpha$ -cyclodextrin in water is 18.5 g/ml,  $\alpha$ -cyclodextrin is not very soluble in TX-100 solutions; the solubility decreases with increasing TX-100 content. These experiments were therefore conducted with by adding lower concentrations of  $\alpha$ -cyclodextrin to the highest concentration of TX-100, 5%, otherwise used and also higher concentrations of  $\alpha$ -cyclodextrin were added to a 0.05% TX-100 solution.

Addition of  $\alpha$ -cyclodextrin in soap solution decidedly changed the transport results as shown in Figure 3.32. Addition of 5 %  $\alpha$ -cyclodextrin to 0.05% TX-100 resulted in a higher  $C/C_0$  and flux of transfer, is the latter being about 2.5 nmol/cm<sup>2</sup>min. Most importantly the (+) form of  $\alpha$ -pinene was preferentially transported, with higher the content of  $\alpha$ -cyclodextrin, higher being the separation factor.

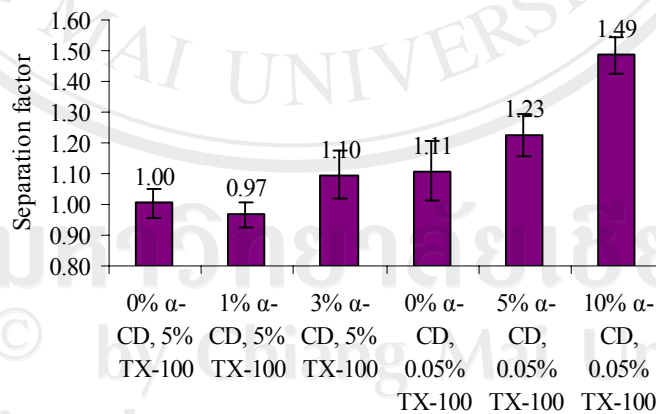
With adding 10%  $\alpha$ -cyclodextrin in soap solution, the one interesting fact was observed: separation factor increase not only in receiver part, but also in donor part, as shown in Figure 3.33. It is possible that  $\alpha$ - pinene which dissolved in TX-100 micelle may move to air-liquid boundary of both donor and receiver parts. As a result when the flow was halt during SPME sampling,  $\alpha$ - pinene molecule concentrated in the liquid film may release back to air phase of the donor part as well.



(a)



(b)



(c)

Figure 3.32 Effect of  $\alpha$ -cyclodextrin content (0-3 %  $\alpha$ -CD in 5% TX-100 + 10% glycerol and 0-10% CD in 0.05% TX-100 + 10% glycerol). a)  $C/C_0$ , b) transfer flux c) separation factor

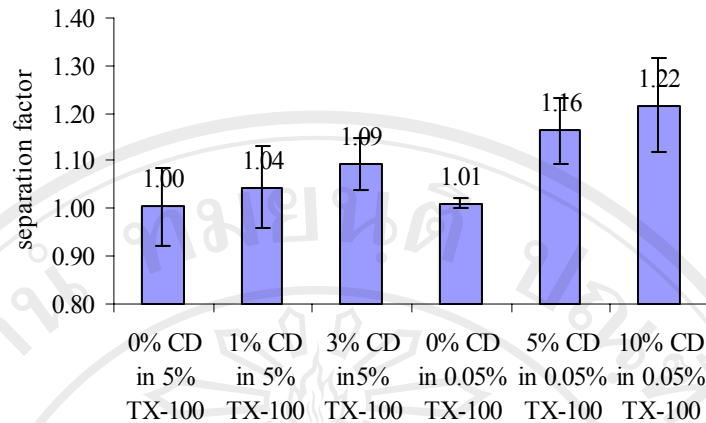


Figure 3.33 Separation factor of  $\alpha$  pinene in donor compartment

### 3.5.5 Effect of transport duration

The transport experiment was carried out with a film of 10%  $\alpha$ -cyclodextrin in 0.05% TX-100 for various lengths of time; the results are shown in Figure 3.34. There is no flow on the receiver side, thus longer the experimental period, the higher is  $C/C_0$ . As a result, the concentration gradient decreases during the experiment and the average transfer flux decreases with increasing experimental duration. It will be expected that the separation factor will decrease over time, this too is observed.

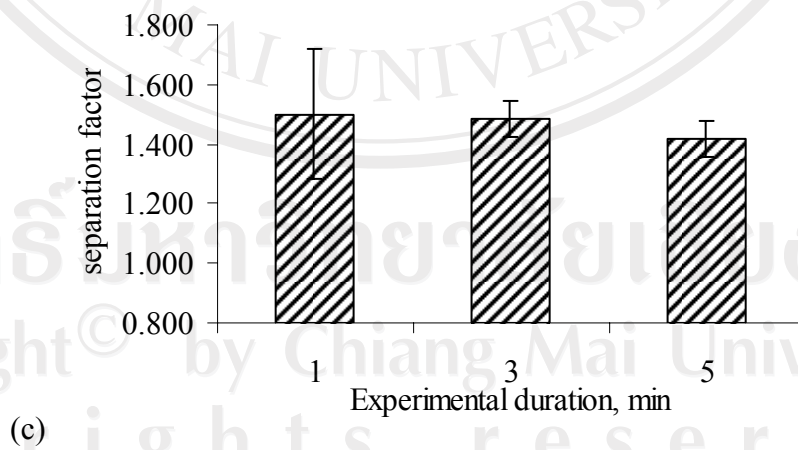
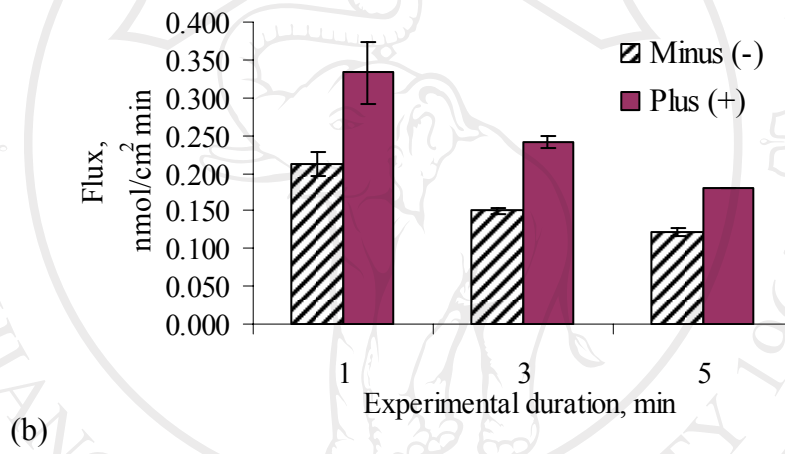
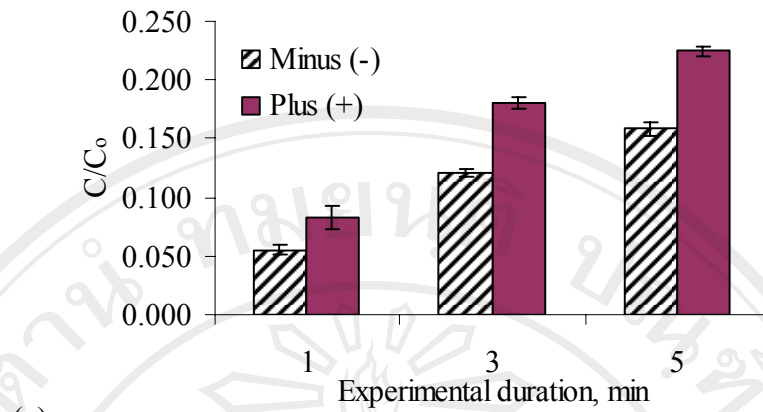


Figure 3.34 Effect of experimental duration on a)  $C/C_0$ , b) transfer flux c) separation factor